Available online at www.sciencedirect.com
ScienceDirect
Icarus 188 (2007) 345–355
ICARUS
www.elsevier.com/locate/icarus

Enceladus: Present internal structure and differentiation by early and long-term radiogenic heating

Gerald Schubert [a,b,*], John D. Anderson [c], Bryan J. Travis [d], Jennifer Palguta [a]

[a] *Department of Earth and Space Sciences, University of California, 595 Charles E. Young Drive East, Los Angeles, CA 90095-1567, USA*
[b] *Institute of Geophysics and Planetary Physics, University of California, 603 Charles E. Young Drive East, Los Angeles, CA 90095-1567, USA*
[c] *Global Aerospace Corporation, 711 West Woodbury Road, Suite H, Altadena, CA 91001-5327, USA*
[d] *Earth & Environmental Sciences Division, EES-2/MS-F665, Los Alamos National Laboratory, Los Alamos, NM 87545, USA*

Received 30 May 2006; revised 27 November 2006

Available online 8 January 2007

Abstract

Pre-Cassini images of Saturn's small icy moon Enceladus provided the first indication that this satellite has undergone extensive resurfacing and tectonism. Data returned by the Cassini spacecraft have proven Enceladus to be one of the most geologically dynamic bodies in the Solar System. Given that the diameter of Enceladus is only about 500 km, this is a surprising discovery and has made Enceladus an object of much interest. Determining Enceladus' interior structure is key to understanding its current activity. Here we use the mean density of Enceladus (as determined by the Cassini mission to Saturn), Cassini observations of endogenic activity on Enceladus, and numerical simulations of Enceladus' thermal evolution to infer that this satellite is most likely a differentiated body with a large rock-metal core of radius about 150 to 170 km surrounded by a liquid water–ice shell. With a silicate mass fraction of 50% or more, long-term radiogenic heating alone might melt most of the ice in a homogeneous Enceladus after about 500 Myr assuming an initial accretion temperature of about 200 K, no subsolidus convection of the ice, and either a surface temperature higher than at present or a porous, insulating surface. Short-lived radioactivity, e.g., the decay of ^{26}Al, would melt all of the ice and differentiate Enceladus within a few million years of accretion assuming formation of Enceladus at a propitious time prior to the decay of ^{26}Al. Long-lived radioactivity facilitates tidal heating as a source of energy for differentiation by warming the ice in Enceladus so that tidal deformation can become effective. This could explain the difference between Enceladus and Mimas. Mimas, with only a small rock fraction, has experienced relatively little long-term radiogenic heating; it has remained cold and stiff and less susceptible to tidal heating despite its proximity to Saturn and larger eccentricity than Enceladus. It is shown that the shape of Enceladus is not that of a body in hydrostatic equilibrium at its present orbital location and rotation rate. The present shape could be an equilibrium shape corresponding to a time when Enceladus was closer to Saturn and spinning more rapidly, or more likely, to a time when Enceladus was spinning more rapidly at its present orbital location. A liquid water layer on Enceladus is a possible source for the plume in the south polar region assuming the survivability of such a layer to the present. These results could place Enceladus in a category similar to the large satellites of Jupiter, with the core having a rock-metal composition similar to Io, and with a deep overlying ice shell similar to Europa and Ganymede. Indeed, the moment of inertia factor of a differentiated Enceladus, C/MR^2, could be as small as that of Ganymede, about 0.31.

Keywords: Enceladus; Interiors; Saturn, satellites

1. Introduction

Enceladus is one of Saturn's two small satellites discovered by W. Herschel in 1789, the other being Mimas. The two satellites are in the 400 to 500 km diameter size range. Both orbit relatively close to Saturn, but at distances well outside the ring system such that they are clearly visible in a small telescope. Saturn's radius, R_S, is about 60,268 km, the A ring ends at about 2.27 R_S, the orbit of Mimas is at about 3.22 R_S, and the orbit of Enceladus is at about 3.95 R_S. However, Earth-based observations of these two satellites are not sufficient for determining their interior properties. Consequently, the data returned

* Corresponding author. Fax: +1 (310) 825 2779.
E-mail address: schubert@ucla.edu (G. Schubert).

0019-1035/$ – see front matter
doi:10.1016/j.icarus.2006.12.012

by Cassini are invaluable for constraining models of Enceladus' internal structure.

Knowledge of the bulk density of a body places a strong constraint on its composition and internal structure. Pre-Cassini studies determined that Enceladus had a mean density suggestive of a composition of mostly water ice with little rock or metal content (Campbell and Anderson, 1989; Peale, 1999). Prior to the Cassini mission, the masses of small satellites such as Enceladus were obtained by measuring long-term orbital motions and by taking advantage of orbit–orbit resonances within the satellite system. The Enceladus–Dione orbital resonance, which can be used to infer the mass of Enceladus, had been considered by Kozai (1957, 1976) using classical perturbation theory. That work obtained a GM for Enceladus of 4.9 ± 2.4 km^3 s^{-2}. The same resonance was considered more recently by Jacobson (2004), with the inclusion of all useful ground-based and spacecraft measurements prior to Cassini, but the dynamics of the satellite interactions were handled by a numerical integration of the equations of motion for the entire Saturn system over the time interval of the observations, September 1966 to December 2003. The resulting GM for Enceladus from that analysis, the best available prior to Cassini, is 6.9 ± 1.5 km^3 s^{-2}, in reasonable agreement with Kozai's result.

Pioneer and Voyager Saturn flybys did not improve on Kozai's estimate of Enceladus' mass (Campbell and Anderson, 1989), so Peale (1999), using the Kozai mass estimate and radius determination from Voyager imaging (Davies and Katayama, 1983), obtained a density for Enceladus of 1120 kg m^{-3} with an uncertainty much too large for reliable geophysical interpretation. Cassini data have reduced the uncertainties in the density to less than 5% (acceptable accuracy for geophysical modeling) and increased Enceladus' density to 1608 ± 5 kg m^{-3}, where the error on the density represents an estimate of the realistic standard deviation (Porco et al., 2006). Unlike previous results, where the mass error dominated the density error budget, the Cassini-determined density is limited by the volume error. The current value for the mean density is higher than the pre-Cassini estimates by about 98 standard deviations. This higher density requires substantially more rock in Enceladus than previously thought. More rock means more radiogenic heat production, a warmer interior, and enhanced likelihood of differentiation of water from rock-metal. Nevertheless, Enceladus' interior state is debated. By assuming hydrostatic equilibrium and using limb measurements, Porco et al. (2006) have determined that Enceladus' shape is inconsistent with a fully differentiated body. However, Porco et al. (2006) do concede that uncertainties in the model allow the possibility that Enceladus might not have a hydrostatic shape. We argue here that Enceladus is not in hydrostatic equilibrium at its present orbital location and spin rate and is likely totally differentiated. Its present shape is consistent with the hydrostatic figure of a more rapidly rotating differentiated Enceladus. Cassini observations of endogenic activity on Enceladus are inconsistent with a primordial, undifferentiated, homogeneous ice–rock interior. We present results of numerical simulations that show how heating by ^{26}Al might fully differentiate a model of Enceladus consisting of a homogeneous ice–rock interior. We also show how long-term radiogenic heating could possibly melt the ice inside an initially homogeneous Enceladus under favorable conditions. Even if ice melting does not occur, long-term radioactivity is shown to warm the ice inside an initially homogeneous Enceladus sufficiently to promote tidal deformation and heating.

2. Density and geologic activity

For smaller satellites and asteroids with low gravity the role of porosity or void space is the major complicating factor in interpreting density information (Anderson et al., 2005). Whether significant porosity exists is also closely connected to a body's ability to maintain a non-spherical shape, because both depend on internal stresses and strengths of material (Johnson and McGetchin, 1973). Satellites with volumes less than approximately 10^{16} m^3 generally have arbitrary and highly irregular shapes, with the ratio a/c of the long axis a to the short axis c ranging from 1.1 to 2.0 (Thomas et al., 1986). Saturn's small satellite Mimas is at the low end of this general rule with a nearly spherical shape (Dermott and Thomas, 1988). Mimas has a mean radius of 198.3 ± 0.6 km (Porco et al., 2006), a volume of 3.27×10^{16} m^3 and appears to have a small mean porosity (Leliwa-Kopystyński and Kossacki, 2000). Enceladus, however, with a mean radius of 252.1 ± 0.2 km (Thomas et al., 2006), has a volume about twice that of Mimas, hence we assume any effects of porosity are negligible. The heating that it apparently underwent is also an argument for neglecting Enceladus' porosity at present day.

The relatively low density of Enceladus suggests a relatively low-density material composition, almost certainly icy. Calculations of rock/ice ratios for Ganymede and Callisto imply an uncompressed density of approximately 1600 kg m^{-3} for the rock–ice material that formed these satellites (Schubert et al., 2004), a density remarkably near Enceladus' density. We assume that Enceladus, like Ganymede and Callisto, is composed of rock-metal and ice. The mass fraction m_c of the rock-metal component, or the ratio of the mass of the rock-metal component to the total mass of Enceladus, follows from the equation

$$\frac{1}{\rho} = \frac{m_c}{\rho_c} + \frac{(1 - m_c)}{\rho_s}, \tag{1}$$

where ρ is the measured mean density, ρ_c is the density of the rock-metal component, and ρ_s is the density of the ice component. If we assume Io's mean density (Schubert et al., 2004) for ρ_c (3527.5 kg m^{-3}), and with some ice contaminants such as CO_2 a density of 1010 kg m^{-3} for ρ_s, Eq. (1) gives $m_c = 0.521 \pm 0.062$, where the standard error reflects reasonable error assumptions on core and shell densities. The assumption of an Io rock-metal mass density for Enceladus accounts for a possible metallic component in Enceladus' composition, and it gives a minimum estimate for the silicate mass fraction. If the rock density is $\rho_c = 2500$ kg m^{-3}, then m_c is about 62%. In the absence of second degree gravity moments, it is impossible to tell how all this material is distributed between the two extremes of a homogeneous satellite and a satellite completely differentiated (ice from rock-metal).

Even without second degree gravity moments, there is evidence that Enceladus is likely totally differentiated. Observations by the Cassini spacecraft have shown Enceladus to be a surprisingly active body. It has been resurfaced, and some areas are so devoid of craters that they must be geologically young (Porco et al., 2006). Systems of ridges, fractures and grooves indicate that the surface has been tectonically altered (Porco et al., 2006). Viscous relaxation of craters has occurred (Porco et al., 2006). Newly discovered dark spots and pits are perhaps indicative of venting of subsurface volatiles (Porco et al., 2006). Enceladus also has an atmosphere which suggests some geologic activity since a sputtered or sublimated atmosphere would be lost due to Enceladus' small size and weak gravity (Dougherty et al., 2006; Hansen et al., 2006; Waite et al., 2006). Furthermore, the south polar region of the satellite contains areas of elevated temperature (Spencer et al., 2006) and is a source of water vapor and ice particles (Spahn et al., 2006). All the above observations require a degree of endogenic activity that would be difficult to reconcile with an interior made of an undifferentiated primordial mixture of ice and rock-metal.

3. Heating by long-lived radioactivity

There is enough rock inside Enceladus that long-lived radioactivity, by itself, could have melted all the ice within the deep interior after several hundred million years. This conclusion depends sensitively on the initial temperature of Enceladus at the end of accretion, whether subsolidus convection or conduction regulated the early thermal evolution of the satellite, the surface temperature of Enceladus during its first 0.5 Gyr of evolution, and the surface thermal conductivity. The last property, which controls how effectively Enceladus can retain its heat, depends strongly on the porosity of the surface. A porous surface can act as an insulator.

Fig. 1 shows the results of thermal conduction calculations for an initially homogeneous Enceladus with silicate mass fractions of 0.52 and 0.60, uniform starting temperatures of 200 and 220 K, and a surface temperature of 170 K. Radial temperature profiles are shown after 400 Myr of heating by long-lived radioactivity and conductive loss of heat to the surface. The calculations assumed a heat source density of 34.5 $\mathrm{W\,kg^{-1}}$ in the rock (Turcotte and Schubert, 2002), constant thermal conductivities of 3 and 2.1 $\mathrm{W\,m^{-1}\,K^{-1}}$ in the rock (Travis and Schubert, 2005) and ice (Grimm and McSween, 1989), respectively, specific heats at constant volume of 692 and 2045 $\mathrm{J\,kg^{-1}\,K^{-1}}$ for rock and ice, respectively (Grimm and McSween, 1989; Ghosh and McSween, 1998; Lide, 2006), and rock density of 3000 $\mathrm{kg\,m^{-3}}$. The temperature in the saturnian nebula during the formation of Enceladus at its present orbital distance from the planet is uncertain, but about 200 K is a plausible value (Ellsworth and Schubert, 1983; Mosqueira and Estrada, 2003). Recent calculations by Canup (private communication) suggest temperatures well in excess of 200 K at the time of Enceladus formation. The possibility of subsolidus convection in a homogeneous ice–rock early Enceladus is also uncertain, but unlikely (Ellsworth and Schubert, 1983).

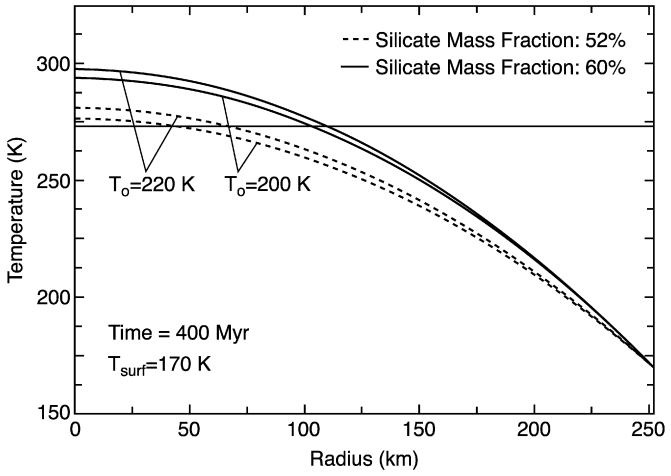

Fig. 1. Temperature vs radius after 400 Myr in a model of Enceladus heated by long-term radioactivity. Heat transfer is by conduction, and the satellite interior is a uniform mixture of ice and rock with silicate mass fractions of 0.52 and 0.60. T_0 is the initial uniform interior temperature. The surface temperature is 170 K. Other parameter values are given in the text.

Fig. 1 shows that the long-lived radiogenic heating raises the temperature of the deep interior of Enceladus above the melting point of ice and warms the ice at shallower depths to temperatures near the melting point. The interior could be warmer than illustrated in Fig. 1 with more ice melting if the surface were porous and insulating. Later in the paper we show how short-lived radioactivity could have completely differentiated Enceladus in just a few million years. The point of the illustrative calculations in Fig. 1 is to emphasize that even without short-lived radioactivity, long-term radiogenic heating can trigger ice melting and differentiation in Enceladus under the right circumstances. These include conditions that mitigate against efficient cooling of the satellite, i.e., a relatively high surface temperature or a porous surface with low thermal conductivity, a warm starting temperature, and no subsolidus convection of the ice. It is reasonable that these conditions existed early in the evolution of Enceladus. Of course, if Enceladus contained a minor constituent like ammonia to reduce the ice melting point, differentiation of its interior is even easier to bring about with just long-lived radiogenic heating.

Although we do not carry out any calculations of tidal heating in this paper, the results of Fig. 1 show that even if the long-lived radioactivity does not melt the ice in Enceladus, it warms it to the point that tidal deformation and heating could become effective in differentiating the satellite. This could help explain the lack of apparent thermal and geologic activity in Mimas, which is closer to Saturn and has a higher eccentricity than Enceladus and therefore should be more strongly tidally heated than Enceladus. However, Mimas is smaller than Enceladus, and it contains a lot less rock. Mimas' density is only about 1148 $\mathrm{kg\,m^{-3}}$ (see Appendix A) and, according to Eq. (1), m_c is between about 0.17 and 0.21, for the same rock densities as assumed for Enceladus. With such a relatively small rock fraction, long-term radiogenic heating is ineffective in warming Mimas to the point where it could be tidally deformed and heated. With the addition of short-lived radioac-

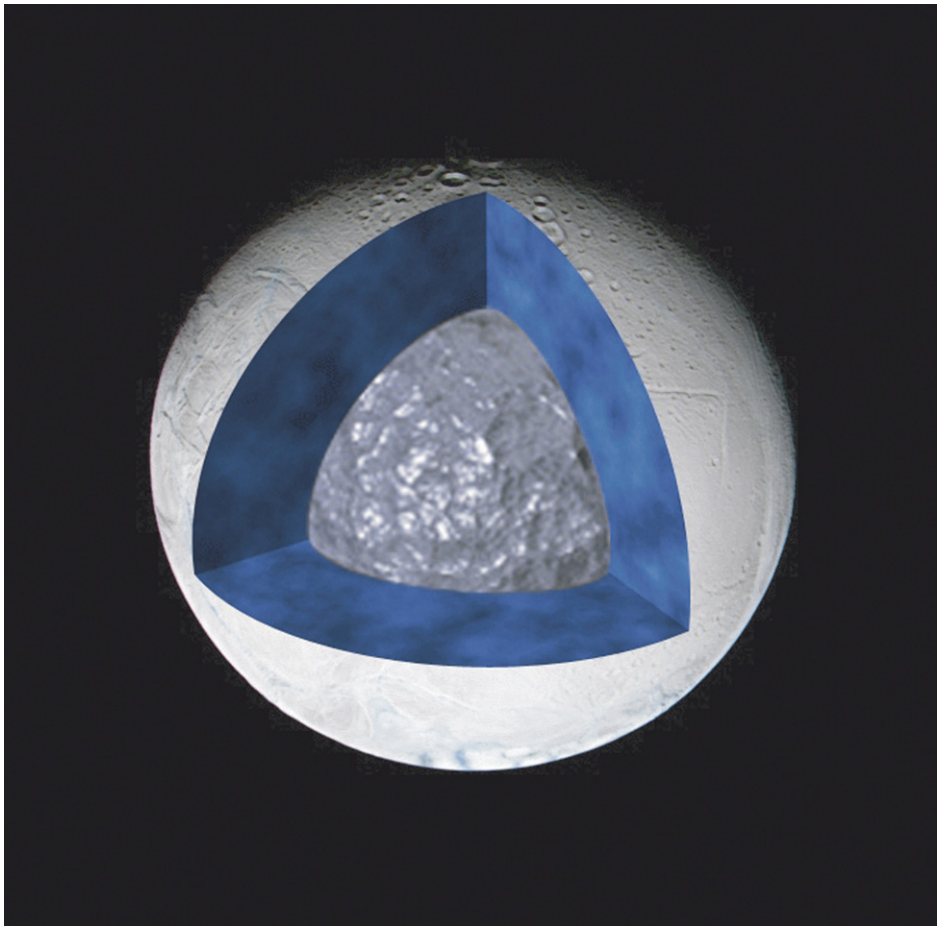

Fig. 2. Illustration drawn to scale of a differentiated Enceladus with a rock-metal core and thick ice shell.

tivity (Matson et al., 2005) and tidal heating it is energetically plausible that the ice and rock inside Enceladus have separated.

4. Core radius and ice–liquid water shell thickness

For the two-layer model, the basic parameter is the ratio β_c of the radius of the rock-metal core to the total radius according to Schubert et al. (2004),

$$\rho = \rho_s + (\rho_c - \rho_s)\beta_c^3. \tag{2}$$

For the rock-metal core density of 3527.5 kg m^{-3} and the ice–liquid water shell density of 1010 kg m^{-3}, β_c is equal to 0.619. In a completely differentiated model with these densities, a rock-metal core extends from the center of Enceladus to a mean radius of about 156 km, and an overlying ice–liquid water shell extends to the surface, about 252 km from the center (see Fig. 2). This corresponds to an ice–liquid water shell thickness of about 96 km. The density of the rock-metal core could plausibly be smaller than the mean density of Io, for example low-density hydrated silicate, but it is unlikely to be larger. The probability distribution function about the mean value of 3527.5 kg m^{-3} is skewed in favor of smaller values. A plot of the thickness of the ice–liquid water shell for a wide range of core densities is shown in Fig. 3. Even though there is a large uncertainty in the density of Enceladus' rock-metal component, the rock fraction and ice–liquid water shell thickness are relatively well determined.

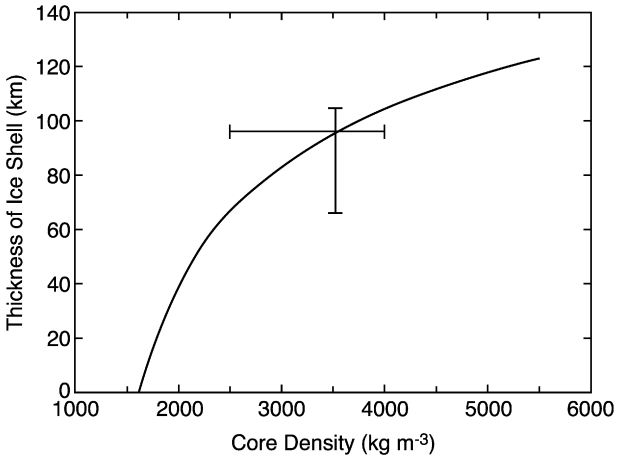

Fig. 3. Plot of ice shell thickness as a function of core density. An estimate of core density is the Io mean density of 3527.5 kg m^{-3} with a corresponding ice–water shell thickness of 96 km. The error bars represent reasonable one-sigma limits on the core density from a minimum of 2500 kg m^{-3} to a minimum of 4000 kg m^{-3}.

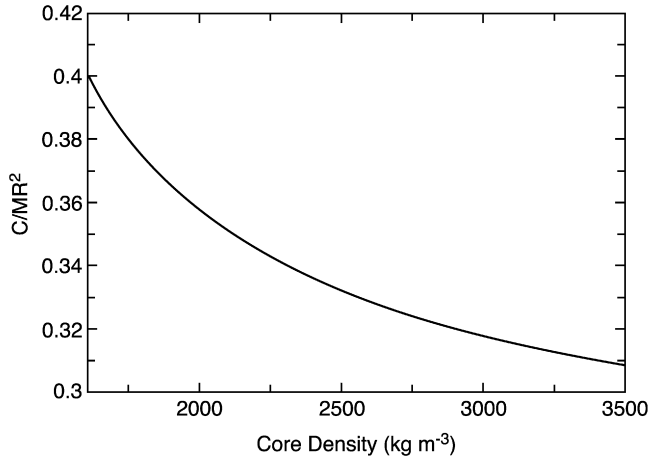

Fig. 4. The moment of inertia factor C/MR^2 as a function of core density for $\rho_s = 1010\ \mathrm{kg\,m^{-3}}$ in a 2-layer model of Enceladus.

5. Moment of inertia

For the fully differentiated model of Enceladus with $\rho_c = 3527.5\ \mathrm{kg\,m^{-3}}$ and $\rho_s = 1010\ \mathrm{kg\,m^{-3}}$, the moment of inertia factor, given by Schubert et al. (2004) as

$$\frac{C}{MR^2} = 0.4\left\{\frac{\rho_s}{\rho} + \frac{\rho_c - \rho_s}{\rho}\beta_c^5\right\} \tag{3}$$

is 0.31. In Eq. (3), C is the axial moment of inertia, M is the satellite mass, and R is the satellite radius. For a homogeneous model of Enceladus C/MR^2 is, of course, 0.4. Fully differentiated models of Enceladus with smaller core densities than above would have C/MR^2 values larger than 0.31. For $\rho_c = 2500\ \mathrm{kg\,m^{-3}}$ and $\rho_s = 1010\ \mathrm{kg\,m^{-3}}$, C/MR^2 is about 0.33. Fig. 4 shows C/MR^2 for a range of core densities and $\rho_s = 1010\ \mathrm{kg\,m^{-3}}$. The moment of inertia factor of Enceladus could be as small as that of Ganymede (Schubert et al., 2004).

The interior structure of Enceladus could be revealed more reliably by a measurement of the external gravitational field with Doppler data acquired during a close approach to the satellite. During the four-year Cassini orbiter tour, no flybys of Enceladus are close enough to infer the normalized moment of inertia C/MR^2 from radio Doppler data. However, if a useful extended mission is possible for Cassini, and if it is approved by NASA, Enceladus could once again become a target for one or more close flybys, and if so, a gravity-field measurement could realistically be included among the science objectives.

6. Shape

Data on the shape of Enceladus (Thomas et al., 2006) can be used to check for hydrostatic equilibrium in the differentiated model. For principal axes $a > b > c$, with the long axis a directed toward Saturn, and c the rotation axis, Cassini imaging data (Thomas et al., 2006) yield $a = 256.6$ km, $b = 251.4$ km, and $c = 248.3$ km. The measurement errors are not given for these axes, but the mean radius is given as 252.1 ± 0.2 km and the axes difference $a - c$ as 8.3 ± 0.6 km. Apparently the absolute size of Enceladus is known to about a factor of three more accurately than the axes differences. We adopt an error of 0.6 km on all three axes differences. The axes difference $b - c = 3.1 \pm 0.6$ km. If Enceladus is in equilibrium under rotational and tidal distortion, the ratio of $a - c$ to $b - c$ should be exactly four, to first-order in the rotational distortion (see below and Hubbard and Anderson, 1978). The imaging data indicate that the actual ratio is 2.7 ± 0.6. The deviation from equilibrium is significant (two standard deviations). This suggests that the surface shape is not representative of an equipotential surface corresponding to Enceladus' internal structure whether differentiated or not.

We emphasize that the ratio $(a - c)/(b - c)$ must equal 4 for any satellite in hydrostatic equilibrium independent of its internal structure. This can be seen as follows. From the formulation of Hubbard and Anderson (1978), the shape of the first-order ellipsoidal equilibrium surface is given by

$$r = \frac{c}{2}\left[2 + q_r + 3\alpha q_r - (1 + 3\alpha)q_t \cos^2\phi \sin^2\theta\right], \tag{4}$$

where r is the distance from the center of mass, c is the polar radius, θ is the colatitude measured from the z-axis or polar axis, and ϕ is the longitude measured from the x-axis (toward Saturn). The physical parameters are the smallness parameters q_r for the rotational distortion and q_t for the tidal distortion,

$$q_r = \frac{\omega^2 R^3}{GM},$$
$$q_t = -3\left(\frac{R}{d}\right)^3 \frac{GM_P}{GM}, \tag{5}$$

where G is the gravitational constant, M is the mass of Enceladus, M_P is the mass of Saturn, R is the mean radius of Enceladus, d is the mean orbital distance of Enceladus from Saturn, and ω is the angular velocity of rotation of Enceladus. For a satellite in synchronous rotation with its orbital period, $q_t = -3q_r$. The measure of central condensation is given by the parameter α, which can be related to the normalized axial moment of inertia C by the Radau approximation,

$$\frac{C}{MR^2} = \frac{2}{3}\left[1 - \frac{2}{5}\left(\frac{5}{3\alpha + 1} - 1\right)^{1/2}\right]. \tag{6}$$

By equating the shape from Eq. (4) with the first-order expansion of the ellipsoid in terms of differences in its principal axes, expressions can be derived for both q_r and q_t. In their most basic form, the rotational and tidal response coefficients are determined independently by

$$q_r = \left(\frac{2}{1 + 3\alpha}\right)\left(\frac{b - c}{c}\right),$$
$$q_t = -\left(\frac{2}{1 + 3\alpha}\right)\left(\frac{a - b}{c}\right). \tag{7}$$

The ratio $(a - c)/(b - c)$ follows from Eq. (7) as

$$\frac{a - c}{b - c} = 1 - \frac{q_t}{q_r} \tag{8}$$

and it is independent of α!

From our axial moment of inertia estimate for the differentiated model, a value for α of 0.26 follows from Eq. (6).

With this value of α and the axes differences given above, we find $q_r = 0.014 \pm 0.003$ and $q_t = -0.023 \pm 0.003$. In the model of constant density, α is 0.5 (Hubbard and Anderson, 1978) and the measured shape implies that $q_r = 0.010 \pm 0.003$ and $q_t = -0.017 \pm 0.003$. The shape-determined value of q_t is significantly different between the homogeneous and differentiated models. They differ by 2.2 standard deviations. We emphasize that the ratio q_t/q_r is exactly minus three in any equilibrium model in synchronous rotation, which is consistent with our assertion that the ratio $(a-c)/(b-c)$ is exactly four in any equilibrium body in synchronous rotation. In fact the measured value of the ratio q_t/q_r is equal to -1.7 ± 0.5, which also shows that the measured shape is not consistent with equilibrium theory.

The shape-determined values of q_r and q_t can be compared with the values for the current rotation rate and orbital position of Enceladus. The current period of rotation and revolution is 1.37022 days. With a GM of 7.2096 $\mathrm{km^3\,s^{-2}}$, and the measured mean radius R of 252.1 ± 0.2 km, the current values from Eq. (5) are $q_r = 0.006260 \pm 0.000016$ and $q_t = -0.018779 \pm 0.000048$. The values adopted for the period and GM are not critical since the error is dominated by the error in the measured mean radius. We point out that the difference between the shape-determined value of q_t and its current value is 0.004 for the differentiated model and 0.002 for the homogeneous model. The measured tidal bulge is consistent with both a homogeneous interior and a differentiated interior at the one sigma level. The real discrepancy is in the measured rotational flattening, which is significantly larger than expected for both the homogeneous and differentiated models. Perhaps the shape of Enceladus reflects a more rapid rotation in the past for synchronous rotation closer to Saturn, or perhaps even a more rapid rotation at its present orbital radius. Neither possibility is excluded by the current Cassini data.

Even though we have shown that Enceladus is not in hydrostatic equilibrium at its present orbital location and rotation rate, we compare the measured value of $a-c$ with values inferred from interior structural models that assume hydrostatic equilibrium. We do this to address the argument given by Porco et al. (2006) and Thomas et al. (2006) that Enceladus has a homogeneous interior. Hydrostatic model values of $a-c$ can be calculated from (Dermott, 1979)

$$a - c = \frac{15}{4} H \left(\frac{\omega^2}{\pi G \rho} \right) R, \tag{9}$$

where H for a 2-layer model is given by

$$H = \frac{\left(\frac{2}{5}\right)\left(\frac{\rho}{\rho_c}\right)\left\{1 + \frac{3}{5}\frac{\delta}{\gamma}\left(\frac{r_c}{R}\right)^2\right\}}{\left[\delta + \frac{2}{5}\frac{\rho_s}{\rho_c} - \frac{9}{25}\frac{\delta}{\gamma}\frac{\rho_s}{\rho_c}\left(\frac{r_c}{R}\right)^2\right]} \tag{10}$$

with

$$\delta = \left(\frac{r_c}{R}\right)^3 \left(1 - \frac{\rho_s}{\rho_c}\right), \tag{11}$$

$$\gamma = \frac{2}{5} + \frac{3}{5}\left(\frac{\rho_s}{\rho_c}\right). \tag{12}$$

For a homogeneous model of Enceladus ($\rho_s = \rho_c$), $H = 1$, and evaluation of Eq. (9) gives $a - c = 7.9$ km. For the fully differentiated model of Enceladus with $\rho_c = 3000\ \mathrm{kg\,m^{-3}}$ and $\rho_s = 1000\ \mathrm{kg\,m^{-3}}$, $H = 0.737$, and $a - c = 5.8$ km. Under the assumption of hydrostatic equilibrium at its present orbital location and rotation rate, a homogeneous Enceladus would have an $a-c$ value within 1 standard deviation of the measurement, while a differentiated Enceladus would have $a-c$ about 4 standard deviations from the measured value. It is on this basis that Porco et al. (2006) and Thomas et al. (2006) prefer a homogeneous model of Enceladus.

The measured value of $a-c$ could be consistent with a differentiated model of Enceladus if the shape of the satellite corresponded with an equilibrium shape acquired when Enceladus had a higher rotation rate and was closer to Saturn (recall the discussion above). The rotation rate for a model with $\rho_c = 3000\ \mathrm{kg\,m^{-3}}$ and $\rho_s = 1000\ \mathrm{kg\,m^{-3}}$ would have to have been 1.165 times the present rotation rate of Enceladus corresponding to a distance of about 0.9 of Enceladus' present distance from Saturn. Porco et al. (2006) and Thomas et al. (2006) argue that Enceladus could not have evolved outward from 0.9 of its present distance from Saturn, but that conclusion is model-dependent (Peale, personal communication). It is also possible that the measured value of $a-c$ was set when a differentiated Enceladus was spinning more rapidly at its present orbital location and subsequently spun down to its present synchronous rotation rate, a possibility discussed above. Indeed, based on the above discussion, this may be the more likely possibility since it is the measured rotational flattening that is significantly larger than model predictions while the measured tidal distortion approximately matches model results.

If the observed value of $(a-c)/(b-c)$ is reliably determined, then, as discussed earlier in this section, the shape of Enceladus is not an equilibrium shape for the present conditions, and it cannot provide a constraint on the satellite's internal structure.

7. Numerical simulations of early differentiation by ^{26}Al heating

The results of numerical simulations of Enceladus' thermal evolution further support the idea that Enceladus is a differentiated body. The simulations use a spherical geometry, and the MAGHNUM code to solve the time-dependent governing equations. MAGHNUM solves the mass, momentum and energy conservation equations in spherical coordinates for a self-consistent gravity field. We use temperature-dependent relations for thermal conductivity of ice and water and rock mixtures, and include conduction of heat, as well as latent energy requirements. The Haar equation of state provides properties of water (density, internal energy, enthalpy, viscosity) as a function of temperature and pressure. Processes include thermal diffusion, phase change, settling of particles, radiogenic heating, and parameterized advection. Details of the MAGHNUM computer code are given by Travis et al. (2003) and Travis and Schubert (2005). The numerical model will automatically account for the

various processes. We let the thermodynamics determine where freezing or melting will occur as a function of time.

Enceladus is assumed to have accreted as a uniform mixture of ice and rock with 71% ice fraction and 29% rock fraction and a density of 1608 $\mathrm{kg\,m^{-3}}$ with a radius of 250 km. The values used for the rock density, thermal conductivity and specific heat are 3300 $\mathrm{kg\,m^{-3}}$, 3 $\mathrm{W\,m^{-1}\,K^{-1}}$, and 750 $\mathrm{J\,K^{-1}\,kg^{-1}}$, respectively. Ice and water properties (e.g., specific heat, thermal conductivity, internal energy) are functions of temperature. A radiation boundary condition at the surface leads to a quickly established surface temperature of about 75 K. The radioactive elements ^{26}Al, ^{235}U, ^{238}U, ^{232}Th, ^{40}K, and ^{60}Fe provide heat to drive differentiation. Chondritic ratios are used for each of these radiogenic elements (Cohen and Coker, 2000) and the abundances (mass fractions) (at time of CAI formation) used are 50.0×10^{-8}, 2.64×10^{-8}, 0.86×10^{-8}, 5.21×10^{-8}, 66.0×10^{-8}, and 10.0×10^{-8}, respectively. A range of values for the ^{26}Al abundance has been suggested (Grimm and McSween, 1989; Wilson et al., 1999; Cohen and Coker, 2000; McCord and Sotin, 2005; Travis and Schubert, 2005). Calcium–aluminum inclusions (CAIs) are generally considered among the oldest known objects formed in the Solar System given their high formation time ^{26}Al/^{27}Al ratio (Podosek and Cassen, 1994). The longer the duration between the formation of CAIs and the formation of Enceladus, the less ^{26}Al would be included in the body's interior. A rapid accretion time would correspond to a large amount of ^{26}Al, which would then initially dominate the heating of the body and result in higher temperatures. The abundance of ^{60}Fe at CAI formation is less certain than ^{26}Al, but it has been upgraded recently to higher values, as have ^{26}Al concentrations (Matson et al., 2006a). There are several factors that would have affected the internal heating of Enceladus—the initial ^{26}Al and ^{60}Fe abundances at the time of CAI formation, the time after CAI formation at which Enceladus evolved, the temperature of the material from which Enceladus evolved, heat liberated from chemical reactions as the interior of Enceladus warmed up to the melting point of ice, and heat from collisions with smaller bodies. Fig. 5 corresponds to an Enceladus formation time at 1.6 Myr after CAI formation. Radionuclide concentrations in the simulations are reduced from CAI abundances appropriately.

The half-lives for ^{26}Al, ^{235}U, ^{238}U, ^{232}Th, ^{40}K, and ^{60}Fe are 0.72 Myr, 4.47 Gyr, 710 Myr, 13.86 Gyr, 1.265 Gyr, and 1.5 Myr, respectively. The heats of decay, the energies released when 1 kg of the corresponding radioactive element decays completely, are 1.11×10^{13}, 1.2×10^{13}, 1.16×10^{13}, 1.03×10^{13}, 0.199×10^{13}, and 0.516×10^{13} $\mathrm{J\,kg^{-1}}$.

Our conceptual model is simple. Rock and ice are initially in a uniform, cold mixture, and the rock is present in a distribution of particle sizes, trapped in the ice matrix. Melting progresses outward from the center. As a thin layer of rock/ice reaches the melting temperature of ice due to radiogenic heating, rock particles are freed from the ice matrix, and fall or drift downward through liquid water towards the planetary body's center, building up a mostly rocky mantle and displacing water outward. Processes operating include thermal diffusion, radiogenic decay, ice to water phase change, and rock particle settling. Fluid flow (other than displacement by falling rock particles) is omitted, but the impact of possible fluid flow on the thermal evolution has been included. As ice melts to form liquid water, the Rayleigh number of liquid computational grid cells is computed. Then the Nusselt number–Rayleigh number relationship is used to obtain an effective thermal conductivity for the liquid layer. This results in a greatly enhanced thermal conductivity, by a factor of 1000 to 10,000. Due to the heating from ^{26}Al, the interior ice is close to melting in only about 400,000 years. It then takes one to two million years longer to completely melt the interior ice. During this time rock falls to the center of the body to form a core–mantle interior with most of the water forming the outer layer.

We assume Stokes flow for the settling velocity of different particle sizes. The settling velocity in a low Reynolds number condition is given by

$$v = d^2 \times g \times \frac{\Delta\rho}{(18 \times \mu)}, \tag{13}$$

where d is the particle diameter, g is gravity, $\Delta\rho$ is the difference between particle and fluid density, and μ is the fluid viscosity. For a 1 mm size particle, the settling speed on Enceladus is about 1 $\mathrm{km\,day^{-1}}$ with larger particles falling faster. Settling speeds would be smaller near the center (due to weaker gravity there), but still fast compared to the rate of melting. Consequently, a distance of kilometers (the numerical grid size) could be traversed even at small radii in less than 3 years by all but the smallest of particles. All the rock is assumed to be present as grains of 100 μm to 1 mm or larger so transit time is very short once rock particles are freed by ice melting. Some water remains in the mantle pores and could contribute to hydrothermal circulation and aqueous alteration of the mantle rock.

Fig. 5 shows the state of Enceladus' interior at different times in its thermal evolution. Fig. 5a shows the initial interior state, frozen, with uniform rock and ice volume fractions. By about 385,000 years after start-up (that is, 1.6 Myr after CAI formation plus 385,000 years), Fig. 5b, the interior has warmed to the freezing point. A rocky core has begun to form, and is already about 25 km in radius, surrounded by a thick partially frozen layer of rocky ice. The outer very cold shell is about 15 km thick. By 770,000 years, Fig. 5c, the rocky core has grown to about 135 km. The peak temperature of the core region has increased to almost 350 °C. The H_2O volume fraction of the partially frozen layer above the rocky core has increased to about 88% and is about 2/3 liquid water, 1/3 ice. This region is a 'swiss-cheese' layer of rocky ice riddled with holes, occupied by liquid water. This region is static in the model, but in reality, if this situation developed, the rock–ice matrix might not be able to sustain the overburden pressures and might collapse rapidly, but counteracting this is the fact that ice is buoyant relative to liquid water. We have ignored the volume change that occurs when ice melts to liquid water. By 1.6 Myr, Fig. 5d, the rocky interior's growth is almost complete, at about 155 km radius. Peak core temperature has risen to 760 °C and is still increasing. Rock fraction is down to 5% in the partially melted zone from 155 to 240 km. The outer ice shell is about 10 km

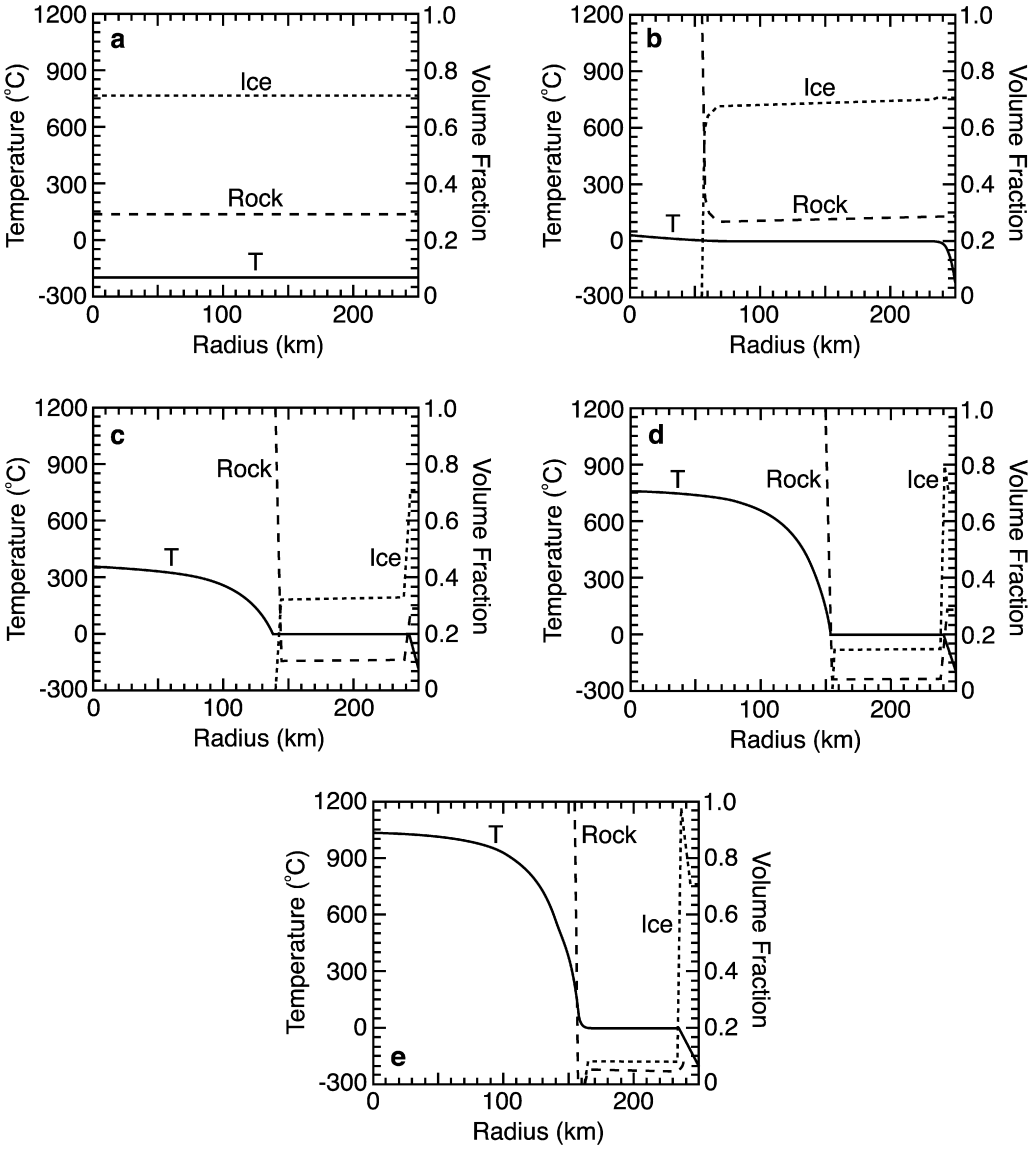

Fig. 5. Five panels showing the computed evolution of a model of Enceladus' interior. The radial temperature profile, rock volume fraction and the ice volume fraction are shown. (a) The initial state, having an ice volume fraction of 71% and a rock volume fraction of 29%. (b) Interior state after about 385,000 years. Some of the interior has warmed up to above-freezing temperatures. A rocky interior out to 55 km radius has begun to form. (c) Interior state after 770,000 years. The rocky interior has grown to about 138 km in radius. Peak temperature has reached 350 °C. (d) The differentiation process is virtually complete by 1.6 Myr. There now exists a hot, rocky interior (155 km radius), a partially frozen layer (80 km), and a 12 km-thick ice shell. Peak temperature is 760 °C. (e) Peak temperature in the core is about 1035 °C at 3.2 Myr. The core/mantle has grown very little since (d). The H_2O between 160 km and 235 km radius is almost melted, having a water volume fraction of about 88%. The ice shell is about 15 km thick.

thick. At 3.2 Myr after start-up, Fig. 5e, the rocky core has grown to 160 km, peak temperature is 1030 °C, and the rock fraction in the melting region (160 to 235 km) is down to 2%. The outer ice shell is now 15 km thick.

The outer partially melted layer above the rocky core and below the outer frozen ice shell remains in a partially frozen state for millions of years. There are competing processes that keep it in this state. It would freeze due to conduction to the very cold surface, but ice that has not melted yet still has radiogenic rock trapped in it, and so has a heat source to slow the rate of cooling. On the other hand, as some ice melts, the trapped rock drops out and falls to the core region. It is no longer available to heat the partially frozen region from which it came. It takes longer and longer for the outer partially frozen layer to warm further, because its internal source of heat is being lost with every additional fraction of melting that occurs. However, conduction from the warmer interior will slow the cooling of the outer partially melted layer. Finally, the latent heat of freezing/melting has to be removed, which further delays the re-freezing of the outer regions.

As mentioned previously, the formation time of Enceladus is uncertain, but recent analysis suggests that Enceladus and Iapetus formed within 3 Myr of CAI formation time (Matson et al., 2006a); Iapetus may have formed within 1–1.6 Myr (Castillo et al., 2005). A second simulation having radionuclide abundances corresponding to 3 Myr after CAI formation still shows

differentiation of the interior of Enceladus. For an accretion time 1.6 Myr after CAI formation (Fig. 5a), about 20% of the initial CAI ^{26}Al abundance remains at start-up. The interior of Enceladus, as shown in Fig. 5, gets very hot and fully differentiates (except for a small amount of rock that remains trapped in the outermost 10 km of the ice shell that never melts in the model). Three million years after CAI formation, only 5.6% of the initial CAI ^{26}Al remains at start-up, yet the interior of Enceladus still differentiates significantly. In this situation, peak temperature reaches about 180 °C, and the rocky core grows to about 120 km. Below an initial ^{26}Al abundance of about 5%, differentiation will not occur, given our assumptions on surface and external temperatures. For example, 3.5 Myr after the time of CAI formation, the initial ^{26}Al abundance is down to 3.4%. At this point, the interior will not melt, unless the initial temperature is considerably higher than 75 K. If the temperature of the contents of Enceladus were at 200 K at the time of Enceladus' formation, then differentiation occurs even at this low abundance, although it is not complete. The peak interior temperature is not nearly as hot as in Fig. 5, but reaches almost to 200 °C, and a significant amount of differentiation occurs, leaving a rocky core of about 115 km radius. Differentiation continues at a very slow rate for several tens of millions of years, as heat from the interior diffuses out into the partially melted H_2O layer, further melting it and releasing more rock. If tidal dissipative heating were to occur, it could essentially finish the differentiation process.

There are several factors that have not been considered that could enhance the differentiation process. (1) Exothermic reactions in the newly formed aqueous phase could add more thermal energy. (2) This study has not considered the presence of salts that could depress the melting temperature. That would enhance the differentiation process, especially at later formation times, when heating is much weaker. Some salts can greatly depress the melting temperature; e.g., eutectic temperature for $CaCl_2$ solution is about −52 °C. (3) Alternatively, NH_3–H_2O mixtures have a low melting point. (4) Tidal dissipative heating would help finish a partially completed differentiation by fairly rapidly melting through the partially frozen H_2O layer above the rocky core, and would insulate the interior against heat loss. Any of these factors would significantly enhance the differentiation process. We have made mid-range to conservative choices of parameter values, so that addition of other processes or discovery of larger values for some parameters would result in even more rapid differentiation. Further, the shape and moment of inertia analyses are consistent with a differentiated interior.

8. Discussion

Our model indicates that it is quite likely that the interior of Enceladus experienced differentiation early in its evolution, due to melting of ice from radiogenic heating, primarily from decay of ^{26}Al. The state of Enceladus at the end of our simulations, some 10 to 20 Myr after formation, is that of a moon with a warm to very hot rocky core of 165 km radius, with a cold liquid ocean roughly 70 km deep, covered by a 15 km ice shell. Admittedly, the jump from that early time to the present day is a long one. Our justification for discussing the current interior of Enceladus lies in other simulations (to be reported elsewhere) that show that the interior can remain above freezing through the action of long-lived radioactivity and tidal dissipative heating for the roughly 4.5 Gyr interval between the formation of Enceladus and the present day. This would not be possible without an early warming and melting period in Enceladus' history, so we believe we are justified in stating that the present-day condition is related to the early time evolution.

Differentiation and the existence of liquid water have important implications for explaining Enceladus' interior and current activity. A layer of liquid water could provide a source for the water-vapor plume detected by Cassini at Enceladus' south polar region (Porco et al., 2006; Spencer et al., 2006). The polar plume is a significant and surprising discovery that has been identified as the source for maintaining Saturn's E ring and a mechanism for resurfacing Enceladus (Hansen et al., 2006). Sublimating ice has been suggested as an alternative to near-surface liquid water as the source for the plumes observed in Enceladus' south polar region. However, sublimation as a source is problematic since the large ice/gas ratio observed by Cassini argues against ice condensing out of vapor as would be expected for sublimation (Porco et al., 2006). Therefore, given the present activity observed by Cassini on Enceladus and the results of the simulations presented above, the possibility that liquid water exists beneath the ice shell should be strongly considered. A major challenge then has been to explain how liquid water could currently exist near Enceladus' surface.

Model simulations show that an initially warm Enceladus could remain above freezing if tidal dissipative heating has occurred. It has been suggested that the orbital eccentricity of Enceladus (0.0047) could be sufficient for substantial tidal heating (Ross and Schubert, 1989; Spencer et al., 2006). However, Mimas has an eccentricity of 0.0202 and no geologic activity has been observed on Mimas despite its higher eccentricity. The density of Enceladus is higher than that of Mimas, indicating that Enceladus contains a greater percentage of rocky material (Castillo et al., 2006). Mimas' density, of only 1148 kg m^{-3}, corresponds to a rock fraction of at most about 20%, less than 1/2 and perhaps only 1/3 that for Enceladus, and the ice mass to rock mass ratio is about three times larger than for Enceladus. Further, Mimas has a 25% higher surface area to volume ratio, meaning that conductive losses to the cold surface will occur more rapidly than for Enceladus. Consequently, stronger radiogenic heating could easily contribute to the differences observed between Mimas and Enceladus. In particular, as already discussed, Mimas could have insufficient rock to warm itself through long-term radiogenic heating to the point where tidal deformation and heating could become effective.

Beyond differentiation, the thermal evolution model presented above suggests the possibility that the interior of Enceladus has been further altered through hydrothermal activity and water–rock reactions. Conditions at the rock–liquid water interface are suitable for geochemical processes. Reactions of water with rocks can affect the oxidation states, mineralogy, organic speciation, ice composition, porosity, morphology, and surface chemistry (Matson et al., 2005; Zolotov, 2005). For ex-

ample, silicate hydration can produce volume changes of the rock which can influence internal and external evolution. Also, the reaction $2NH_3 \rightarrow N_2 + 3H_2$ could explain the N_2 observed among the plume products (Matson et al., 2006b). As with Europa, Enceladus' suitability as a habitat can be investigated. Future modeling can include the relevant hydrothermal circulation and geochemical reactions to explore Enceladus' chemical environment and the amount of metabolic energy that could be produced.

Melting and differentiation of Enceladus could have been facilitated by the presence of ammonia mixed with water. NH_3 has not been identified on Enceladus (Brown et al., 2006; Porco et al., 2006; Waite et al., 2006). However, ammonia–water mixtures may be circulating subsurface (Porco et al., 2006). The water plume might arise from dissociation of clathrate hydrates from which ammonia had been excluded by earlier clathrate formation (Kargel, 2006; Prieto-Ballesteros and Kargel, 2006). Hydrothermal circulation may have also sequestered NH_3 in rocky ammonium minerals. The presence of ammonia suppresses the melting temperature of the ammonia–water ice increasing the likelihood of melting during the thermal evolution of the body (Matson et al., 2005).

There are still many questions about Enceladus' interior. Models for the interior of Enceladus will continue to rely on a variety of data and on models of thermal evolution. It will be a challenge to identify the source or sources of energy for all the activity on this small satellite.

Acknowledgments

A portion of this study was supported by the Cassini Project and was done at the Jet Propulsion Laboratory, California Institute of Technology, under a contract from NASA. G.S. acknowledges support by grants from NASA through the Planetary Geology and Geophysics program. B.J.T. and J.P. acknowledge support from LANL's Institute of Geophysics and Planetary Physics. We thank JPL's Sami W. Asmar and Roberto Aguilar for Fig. 1. We also appreciate informative discussions with Stanton Peale and Frank Sohl.

Appendix A. Density of Mimas

Based on the work of Kozai (1957), who studied the orbital resonance between Mimas and Tethys (see also Blitzer and Anderson, 1981), Campbell and Anderson (1989) derived a value of GM for Mimas of 2.50 ± 0.06 km^3 s^{-2}, where G is the gravitational constant and M is the mass. This was later confirmed by a numerical integration of the entire saturnian system as reported by Jacobson (2004), who obtained a GM of 2.55 ± 0.05 km^3 s^{-2}. The most accurate value of GM was obtained later by a similar numerical integration of the saturnian system, but with additional data from the Cassini mission for a GM determination of 2.5023 ± 0.0020 km^3 s^{-2} (Jacobson et al., 2006). With a modern value for G of $6.674215 \pm 0.000092 \times 10^{-20}$ km^3 s^{-2} kg^{-1} (Gundlach and Merkowitz, 2000), the best estimate for the mass of Mimas is $3.7492 \pm 0.0030 \times 10^{19}$ kg, where the error is dominated by the error in GM, not the error in G. A determination of the bulk density requires an estimate for the total volume of Mimas. From the processing of 16 Cassini images of Mimas, the principal axes (a, b, c) are 207.4, 197.2, and 190.7 km for a mean radius (the cube root of the product abc) of 198.3 ± 0.6 km (Thomas et al., 2006). The resulting volume is $3.266 \pm 0.030 \times 10^{16}$ m^3 and the bulk density is 1147.8 ± 10.5 kg m^{-3}, where the error is dominated by the error in the volume, not the mass.

References

Anderson, J.D., Johnson, T.V., Schubert, G., Asmar, S., Jacobson, R.A., Johnston, D., Lau, E.L., Lewis, G., Moore, W.B., Taylor, A., Thomas, P.C., Weinwurm, G., 2005. Amalthea's density is less than that of water. Science 308, 1291–1293.

Blitzer, L., Anderson, J.D., 1981. Theory of satellite orbit–orbit resonance. Celest. Mech. 29, 65–78.

Brown, R.H., Clark, R.N., Buratti, B.J., Cruikshank, D.P., Barnes, J.W., Mastrapa, R.M.E., Bauer, J., Newman, S., Momary, T., Baines, K.H., Bellucci, G., Capaccioni, F., Cerroni, P., Combes, M., Coradini, A., Drossart, P., Formisano, V., Jaumann, R., Langevin, Y., Matson, D.L., McCord, T.B., Nelson, R.M., Nicholson, P.D., Sicardy, B., Sotin, C., 2006. Composition and physical properties of Enceladus' surface. Science 311, 1425–1428.

Campbell, J.K., Anderson, J.D., 1989. Gravity field of the saturnian system from Pioneer and Voyager tracking data. Astron. J. 97, 1485–1495.

Castillo, J.C., Matson, D.L., Sotin, C., Johnson, T.V., Lunine, J.I., Thomas, P.C., 2005. ^{26}Al in Iapetus—Consequences for the formation of the saturnian system. Eos 86 (Fall Suppl.). Abstract #P21F-02.

Castillo, J.C., Matson, D.L., Sotin, C., Johnson, T.V., Lunine, J.I., Thomas, P.C., 2006. A new understanding of the internal evolution of saturnian icy satellites from Cassini observations. Lunar Planet. Sci. XXXVII. Abstract #2200.

Cohen, B.A., Coker, R.F., 2000. Modeling of liquid water on CM meteorite parent bodies and implications for amino acid racemization. Icarus 145, 369–381.

Davies, M.E., Katayama, F.Y., 1983. The control networks of Mimas and Enceladus. Icarus 53, 332–340.

Dermott, S.F., 1979. Shapes and gravitational moments of satellites and asteroids. Icarus 37, 575–586.

Dermott, S.F., Thomas, P.C., 1988. The shape and internal structure of Mimas. Icarus 73, 25–65.

Dougherty, M.K., Khurana, K.K., Neubauer, F.M., Russell, C.T., Saur, J., Leisner, J.S., Burton, M.E., 2006. Identification of a dynamic atmosphere at Enceladus with the Cassini magnetometer. Science 311, 1406–1409.

Ellsworth, K., Schubert, G., 1983. Saturn's icy satellites: Thermal and structural models. Icarus 54, 490–510.

Ghosh, A., McSween, H.Y., 1998. A thermal model for differentiation of Asteroid 4 Vesta, based on radiogenic heating. Icarus 134, 187–206.

Grimm, R.E., McSween, H.Y., 1989. Water and the thermal evolution of carbonaceous chondrite parent bodies. Icarus 82, 244–280.

Gundlach, J.H., Merkowitz, S.M., 2000. Measurement of Newton's constant using a torsion balance with angular acceleration feedback. Phys. Rev. Lett. 85, 2869–2872.

Hansen, C.J., Esposito, L., Stewart, A.I.F., Colwell, J., Hendrix, A., Pryor, W., Shemansky, D., West, R., 2006. Enceladus' water vapor plume. Science 311, 1422–1425.

Hubbard, W.B., Anderson, J.D., 1978. Possible flyby measurements of Galilean satellite interior structure. Icarus 33, 336–341.

Jacobson, R.A., 2004. The orbits of the major saturnian satellites and the gravity field of Saturn from spacecraft and Earth-based observations. Astron. J. 128, 492–501.

Jacobson, R.A., Antreasian, P.G., Bordi, J.J., Criddle, K.E., Ionasescu, R., Jones, J.B., Mackenzie, R.A., Meek, M.C., Parcher, D., Pelletier, F.J., Owen Jr., W.M., Roth, D.C., Roundhill, I.M., Stauch, J.R., 2006. The gravity field of the saturnian system from satellite observations and spacecraft tracking data. Astron. J. 132, 2520–2526.

Johnson, T.V., McGetchin, T.R., 1973. Topography on satellite surfaces and the shape of asteroids. Icarus 18, 612–620.

Kargel, J.S., 2006. Enceladus: Cosmic gymnast, volatile miniworld. Science 311, 1389–1391.

Kozai, Y., 1957. On the astronomical constants of saturnian satellites system: Titan and Rhea, saturnian satellites, 1927–1947. Ann. Tokyo Obs. 5, 71–127.

Kozai, Y., 1976. Masses of satellites and oblateness parameters of Saturn. Publ. Astron. Soc. Jpn. 28, 675–691.

Leliwa-Kopystyński, J., Kossacki, K.J., 2000. Evolution of porosity in small icy bodies. Planet. Space Sci. 48, 727–745.

Lide, D.R. (Ed.), 2006. CRC Handbook of Chemistry and Physics. CRC Press, Boca Raton, FL, p. 2608.

Matson, D.L., Castillo, J.C., Johnson, T.V., Lunine, J.I., McCord, T.B., Sotin, C., Thomas, P.C., Turtle, E.P., 2005. Thermal evolution models for Enceladus defining the context for the formation of the south pole thermal anomaly. Eos 86 (Fall Suppl.). Abstract #P32A-05.

Matson, D.L., Castillo, J.C., Johnson, T.V., Lunine, J., 2006a. Iapetus and Enceladus: First contributions of high-precision geophysical modeling to Solar System chronometry and chronology. In: Planetary Chronology Workshop 2006. Abstract #6023.

Matson, D.L., Castillo, J.C., Sotin, C., Johnson, T.V., Lunine, J.I., Davies, A.G., McCord, T.B., Thomas, P.C., Turtle, E.P., 2006b. Enceladus' interior and geysers—Possibility for hydrothermal geochemistry and N_2 production. Lunar Planet. Sci. XXXVII. Abstract #2219.

McCord, T.B., Sotin, C., 2005. Ceres: Evolution and current state. J. Geophys. Res. 110, doi:10.1029/2004JE002244. E05009.

Mosqueira, I., Estrada, P.R., 2003. Formation of the regular satellites of giant planets in an extended gaseous nebula. I. Subnebula model and accretion of satellites. Icarus 163, 198–231.

Peale, S.J., 1999. Origin and evolution of the natural satellites. Annu. Rev. Astron. Astrophys. 37, 533–602.

Podosek, F.A., Cassen, P., 1994. Theoretical, observational, and isotopic estimates of the lifetime of the solar nebula. Meteoritics 29, 6–25.

Porco, C.C., Helfenstein, P., Thomas, P.C., Ingersoll, A.P., Wisdom, J., West, R., Neukum, G., Denk, T., Wagner, R., Roatsch, T., Kieffer, S., Turtle, E., McEwen, A., Johnson, T.V., Rathbun, J., Veverka, J., Wilson, D., Perry, J., Spitale, J., Brahic, A., Burns, J.A., DelGenio, A.D., Dones, L., Murray, C.D., Squyres, S., 2006. Cassini observes the active south pole of Enceladus. Science 311, 1393–1401.

Prieto-Ballesteros, O., Kargel, J.S., 2006. Clathration as a process for the cryomagmatic differentiation of icy satellites: Application to Enceladus and Europa. Lunar Planet. Sci. XXXVII. Abstract #1971.

Ross, M.N., Schubert, G., 1989. Viscoelastic models of tidal heating in Enceladus. Icarus 78, 90–101.

Schubert, G., Anderson, J.D., Spohn, T., McKinnon, W.B., 2004. Interior composition, structure and dynamics of the Galilean satellites. In: Bagenal, F., Dowling, T.E., McKinnon, W.B. (Eds.), Jupiter: The Planet, Satellites and Magnetosphere. Cambridge Univ. Press, Cambridge, pp. 281–306.

Spahn, F., Schmidt, J., Albers, N., Hörning, M., Makuch, M., Seiß, M., Kempf, S., Srama, R., Dikarev, V., Helfert, S., Moragas-Klostermeyer, G., Krivov, A.V., Sremčević, M., Tuzzolino, A.J., Economou, T., Grün, E., 2006. Cassini dust measurements at Enceladus and implications for the origin of the E ring. Science 311, 1416–1418.

Spencer, J.R., Pearl, J.C., Segura, M., Flasar, F.M., Mamoutkine, A., Romani, P., Buratti, B.J., Hendrix, A.R., Spilker, L.J., Lopes, R.M.C., 2006. Cassini encounters Enceladus: Background and the discovery of a south polar hot spot. Science 311, 1401–1405.

Thomas, P., Veverka, J., Dermott, S., 1986. Small satellites. In: Burns, J.A., Matthews, M.S. (Eds.), Satellites. Univ. of Arizona Press, Tucson, AZ, pp. 802–835.

Thomas, P.C., Veverka, J., Helfenstein, P., Porco, C., Burns, J., Denk, T., Turtle, E., Jacobson, R.A., the ISS Science Team, 2006. Shapes of the saturnian icy satellites. Lunar Planet. Sci. XXXVII. Abstract #1639.

Travis, B.J., Schubert, G., 2005. Hydrothermal convection in carbonaceous chondrite parent bodies. Earth Planet. Sci. Lett. 240, 234–250.

Travis, B.J., Rosenberg, N.D., Cuzzi, J.N., 2003. On the role of widespread subsurface convection in bringing liquid water close to Mars' surface. J. Geophys. Res. 108 (E4), doi:10.1029/2002JE001877. 8040.

Turcotte, D.L., Schubert, G., 2002. Geodynamics. Cambridge Univ. Press, Cambridge, UK. 472 pp.

Waite, J.H., Combi, M.R., Ip, W.-H., Cravens, T.E., McNutt, R.L., Kasprzak, W., Yelle, R., Luhmann, J., Niemann, H., Gell, D., Magee, B., Fletcher, G., Lunine, J., Tseng, W.-L., 2006. Cassini ion and neutral mass spectrometer: Enceladus plume composition and structure. Science 311, 1419–1422.

Wilson, L., Keil, K., Browning, L.B., Krot, A.N., Bourcier, W., 1999. Early aqueous alteration, explosive disruption, and reprocessing of asteroids. Meteorit. Planet. Sci. 34, 541–557.

Zolotov, M.Y., 2005. Water–rock reactions on non-planetary bodies in the early Solar System. Eos 86 (Fall Suppl.). Abstract #P53A-07.